Cell, Vol. 91, 447–456, November 14, 1997, Copyright ©1997 by Cell Press

The Structure of ClpP at 2.3 Å Resolution Suggests a Model for ATP-Dependent Proteolysis

Jimin Wang,† James A. Hartling,* and John M. Flanagan*‡
*Biology Department
Brookhaven National Laboratory
Upton, New York 11973-5000
†Department of Molecular Biophysics and Biochemistry
Yale University
New Haven, Connecticut 06520-8114

Summary

We have determined the crystal structure of the proteolytic component of the caseinolytic Clp protease (ClpP) from E. coli at 2.3 Å resolution using an ab initio phasing procedure that exploits the internal 14-fold symmetry of the oligomer. The structure of a ClpP monomer has a distinct fold that defines a fifth structural family of serine proteases but a conserved catalytic apparatus. The active protease resembles a hollow, solid-walled cylinder composed of two 7-fold symmetric rings stacked back-to-back. Its 14 proteolytic active sites are located within a central, roughly spherical chamber ~51 Å in diameter. Access to the proteolytic chamber is controlled by two axial pores, each having a minimum diameter of ~10 Å. From the structural features of ClpP, we suggest a model for its action in degrading proteins.

Introduction

Protein degradation in all living cells is essential for eliminating abnormal proteins and for the temporal control of many cellular processes involving short-lived regulators. Surprisingly, though peptidyl hydrolysis is an exergonic process, most protein degradation in cells is carried out by a few large, energy-dependent proteases. For example, in Escherichia coli, Lon and Clp account for up to 80% of protein degradation (Maurizi, 1992; Goldberg et al., 1994) with additional contributions from HslUV (also known as ClpYQ) and FtsH (Tomoyasu et al., 1995; Wawrzynow et al., 1995). The soluble ATP-dependent proteases fall into three archetypal families: Lon (La), Clp (Ti), and the 26S proteasome (Goldberg, 1990, 1992; Coux et al., 1996; Gottesman, 1996). All of these ATP-dependent proteases share the same barrel-shaped architecture and may have similar biochemical mechanisms (Kessel et al., 1995; Koster et al., 1995; Lupas et al., 1997; Rohrwild et al., 1997). Recently, the structures of the proteolytic core (20S proteasomes) of the yeast (Groll et al., 1997) and Thermoplasma acidophilum (Lowe et al., 1995) 26S proteasomes, and the proteolytic component, HslV, from E. coli HslUV (Bochtler et al., 1997) were determined to 3.4 and 2.4 Å and 3.8 Å, respectively. The subunits of these oligomers share a common fold, although their quaternary associations are different: the 20S proteasomes are composed of 4 heptameric rings while HslV has 2 hexameric rings. Here, we report the 2.3 Å resolution crystal structure of the proteolytic component of the E. coli Clp protease, ClpP.

The functional Clp protease is comprised of two components: a proteolytic component, ClpP, and one of several regulatory ATPase components. The two components associate in an ATP-dependent manner with the ATPase subunits conferring substrate specificity and activating ClpP for proteolysis (Gottesman et al., 1997). In E. coli, ClpA (Hwang et al., 1988; Katayama et al., 1988) and ClpX (Gottesman et al., 1993; Wawrzynow et al., 1995) are the regulatory components of Clp, while in other organisms ClpC may be the evolutionary equivalent of ClpA (Shanklin et al., 1995). Homologs of ClpP and the ATPase components of Clp have been identified in the genomes of most bacteria, human mitochondria, and plant plastids. In E. coli, the in vivo substrates of Clp include abnormal proteins and several short-lived regulatory proteins. For example, alone, ClpP degrades the model substrate CRAG by a novel pathway involving Trigger Factor and GroEL (Kandror et al., 1994); with ClpA, ClpP degrades some β-galactosidase fusion proteins by a pathway that depends upon the nature of the residue at their amino termini (Tobias et al., 1991), and MazE, an endogenous regulator of programmed cell death (Aizenman et al., 1996); with ClpX, ClpP degrades some proteins involved in replication, transcription, and translational control, such as the λ-O protein (Wojtkowiak et al., 1993), the phage P1 protein, Phd (Lehnherr and Yarmolinsky, 1995), and the σ factor RpoS (Schweder et al., 1996). The three known ATPase components of Clp are members of the Clp/Hsp100 family of molecular chaperones (reviewed in Squires and Squires, 1992; Wawrzynow et al., 1996; Gottesman et al., 1997), with ClpA and ClpC containing two Walker consensus ATP-binding motifs and ClpX only a single motif. Electron microscopic studies of E. coli ClpA suggest that it is hexameric and point to a symmetry mismatch in the ClpAP complex (Kessel et al., 1995). Similar symmetry mismatches may also exist in HslUV and in the 26S proteasome (Koster et al., 1995; Rohrwild et al., 1997). The ATPase subunits of Clp function both in proteolysis and as molecular chaperones in several cellular reactions (Squires and Squires, 1992; Horwich, 1995; Wawrzynow et al., 1996; Gottesman et al., 1997), including protein import into plant plastids (Nielsen et al., 1997), activation of the phage P1 RepA protein (Wickner et al., 1994), and assembly of the Mu transposase (Levchenko et al., 1995). The ability of the Clp ATPase subunits to participate both in protein folding/remodeling and in protein degradation reactions suggests a role for the Clp protease in protein quality control in the cell.

ClpP is synthesized as a 207-residue proprotein that is autoproteolytically processed to yield the mature 193-residue protein during folding/assembly (Maurizi et al., 1990; we have numbered the sequence according to mature ClpP). Native ClpP exists as a stable tetradecamer composed of two rings of seven subunits each (Flanagan et al., 1995; Kessel et al., 1995; Shin et al.,

‡To whom correspondence should be addressed.

1996); it displays limited serine-peptidase activity against peptides of fewer than 6 residues, preferentially cleaving them after hydrophobic residues (Woo et al., 1989; Maurizi et al., 1994). Ser-97 and His-122 were identified by mutagenesis as two components of its catalytic triad (Maurizi et al., 1990); in this study, we have identified Asp-171 as the third component. Degradation of peptides longer than ~6 residues requires the participation of an ATPase subunit such as ClpA to form the active protease (ClpAP), but not ATP hydrolysis; by contrast, degradation of protein substrates requires ATP hydrolysis as well as ClpAP. Protein substrates are degraded in a highly processive manner, producing 7- to 10-residue peptides; the pattern of cleavage does not show any clear sequence specificity (Maurizi et al., 1994; Thompson and Maurizi, 1994; Thompson et al., 1994). At present, little is known about the mechanism of ATP-dependent proteolysis by Clp; from the crystal structure of ClpP presented here, we provide some essential structural clues to its mechanism of action.

Results and Discussion

Structure Determination

The crystals of ClpP diffract to 2.2 Å resolution and belong to the space group C2 with cell dimensions: a = 193.32 Å, b = 102.46 Å, c = 157.08 Å, and β = 97.8°. The asymmetric unit contains a single tetradecamer and has an estimated solvent content of 55% (Matthews, 1968). The structure of ClpP was determined without the benefit of heavy atom derivatives, utilizing instead the 14-fold NCS (noncrystallographic symmetry) information present in the diffraction data. Initial phases were calculated from a cylindrically symmetric molecular mask, determined from electron microscopy and solution small-angle scattering. The 7-fold NCS matrices, determined from the self-rotation function, allowed the phases to be refined and gradually extended from 20 to 8 Å resolution. Conceptually, this procedure is analogous to molecular replacement followed by NCS averaging, solvent flattening, and phase extension to high resolution. However, it differs from molecular replacement in at least one key aspect: the rather crude uniform density model for ClpP is only valid at sufficiently low resolution, where the phases of diffraction data depend primarily on the overall shape of the particle, its orientation and location, and the solvent content in the unit cell, and are much less dependent on fluctuations in electron density within the mask (or object). The additional 2-fold axes were identified in electron density maps calculated at 8 Å resolution, allowing 14-fold averaging to be used in subsequent phase refinement and extension to 2.2 Å resolution. At 5 Å resolution, the map showed some inconsistencies with the starting molecular mask. The mask was changed to reflect the new experimental density, and thereafter, it was continuously improved with maskless averaging and the NCS operators were updated. The phase refinement and extension procedure yielded an experimental electron density map at 2.2 Å resolution (Figure 1) that was readily interpretable; even ordered solvent molecules were clearly visible. A model was built and refined using standard techniques (Table 1).

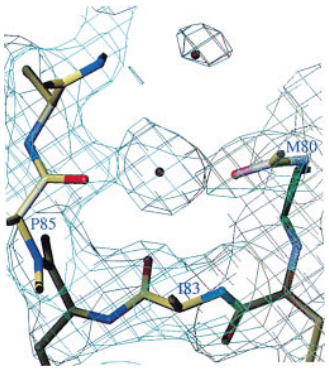

Figure 1. Electron Density Map of the Region between Helix C and Strand 5

The $|F_o|\exp(i\varphi^{ave})$ electron density map is contoured at 1.5 σ and superimposed upon the refined model. |Fo| and φ^{ave} are the observed amplitudes, and the calculated phases after NCS averaging with RAVE (Jones, 1992), respectively. In this map, the turn between helix C and strand 5 (residues 80–85) is stabilized by a solvent molecule or a cation. The refined model is superimposed on the density as a wire model. A water molecule and the unidentified solvent/cation molecule are shown as magenta spheres.

ClpP Subunits Have a Unique Fold around a Conserved Serine

Protease Architecture

Each ClpP subunit has an α/β fold made up of six repeats of the α/β unit (A/1/2, B/3/4, C/5/6, D/7/8, F/10, and G/11) with an additional protruding α/β unit (E/9). The ten β strands (1–8, 10, and 11) form two layers of β sheets that pack against a layer of α helices (A–D and F, G). The layers of sheets are mutually perpendicular, creating one side of the substrate-binding cleft. In projection, the ClpP monomer resembles a hatchet with a wedge-shaped head (head domain) and a short handle (Figures 2A and 2B). Residues 28–120 and 160–188 comprise the head domain, and the "handle" is formed by residues 125–130 and 132–157 (β strand 9 and helix E). The amino (residues 11–27) and carboxyl (189–193) termini lie at opposite ends of the head domain, extending away from its central core. The catalytic triad, Ser-97, His-122, and Asp-171, is located in a cleft at the junction of the head domain and handle (Figures 2A and 2B). The secondary structural elements are shown in Figure 2C above a sequence alignment of members of the ClpP family.

It is our belief that the structure of ClpP defines a fifth family of serine proteases (the other four being chymotrypsin-like, trypsin-like, subtilisin-like, and Cytomegalovirus proteases; Perona and Craik, 1995; Chen et al., 1996) and represents a new fold; comparison with proteins in the DALI database (Holm and Sander, 1993) revealed only a weak similarity between the three-dimensional structures of ClpP and porcine ribonuclease inhibitor (Kobe and Deisenhofer, 1993), a functionally unrelated protein. Although the tertiary folds of the five serine protease families are distinct, the essential features of their catalytic architecture are conserved. This is evident in a least-squares superposition of the active sites of ClpP and trypsin (Figure 3A) that allowed us to identify Asp-171, 1 of 8 conserved negatively

Table 1. Summary of Crystallographic Data

Data Collection Statistics for Data Used in Structure Solution				
Data Sets	Resolution (Å)	Completeness (%)	Number of Reflections	R_{merge} (%)
LOWRES	80–4.0	96	23,675	15.5
HIGHRES	41–2.2	92.5	142,415	3.7
	2.3–2.2	75.5	11,607	17.7
COMBIN	80–2.2	93.3	142,952	7.7

Structure Refinement		
Number of protein atoms	20,062	
Number of solvent molecules	1,246	
Number of reflections (5.0–2.3 Å with 2 σ cutoff)	120,272	
Number of reflections (80–2.3 Å with 2 σ cutoff)	131,572	
Rms bond deviation (Å)‡	0.008 Å	
Rms angle deviation (°)‡	1.53°	
Final R factor (80–2.3 Å)	21.9%	R_{free} = 29.2%

Standard definitions are used for all of the parameters (Drenth, 1994). The values for the data collection statistics are taken from SCALEPACK (Otwinowski and Minor, 1997), and the values for the refinement and geometric statistics are taken from X-PLOR (Brünger, 1992). The Ramachandran analysis was performed with PROCHECK (Laskowski et al., 1993). Both native sets (COMBIN) were combined with a 1 σ cutoff for intensities. Excluding these reflections allowed us to extend and refine the phases to the 2.2 Å resolution limit. For the combined native data set, the R_{merge} was 22.5% for the data between 80 and 4.5 Å resolution.

charged residues, as the third component of the triad. In the refined structure of ClpP, a hydrogen bond between Asp-171 and His-122 is evident: the distance between the Asp-171Oδ1 and His-122Nδ1 is 2.9 Å and the expected hydrogen bond is nearly colinear in the Oδ1-H-Nδ1 arrangement. Additionally, the side chain of Asp-171 forms two hydrogen bonds with the side chains of the nonconserved residues His-138 and Tyr-128, both of which are contributed by a neighboring intraring subunit. A similar arrangement is observed in chymotrypsin where the orientation of the catalytic aspartate is fixed by a hydrogen bond involving the backbone amide of the catalytic histidine (Blow and Steitz, 1970). Consistent with a role for Asp-171 in the catalytic triad, ClpP where Asp-171 is substituted with alanine lacks peptidase activity against a fluorogenic peptide (K. Griffin and J. M. F. unpublished data).

In the apo structure of ClpP, the catalytically important hydrogen bond between Ser-97Oγ-His-122Nϵ2 is not present. Although the Nϵ2-Oγ distance is 2.7 Å, the angular geometry of the resultant hydrogen bond would be poor (Figure 3A). Mechanistic studies in some serine proteases indicate that this interaction is absent in the resting state and forms only during hydrolysis of peptide bonds (Steitz and Shulman, 1982). To characterize further the serine proteolytic mechanism of ClpP, we determined the structure of a covalent complex between ClpP and di-isopropyl-fluorophosphate (DFP) at 2.5 Å resolution. In a difference Fourier map (2Fo − Fc[apo]), electron density was observed in all 14 active sites corresponding to a covalent adduct between Ser-97Oγ and di-isopropyl-phosphate. In the complex, the backbone amides of Gly-68 and Met-98, which are thought to participate in stabilization of the oxyanion intermediate, are hydrogen-bonded to an oxygen atom of the phosphate (Figure 3B); the Oγ of Ser-97 reorients, forming a covalent attachment to this phosphate; and His-122Nϵ2 forms a hydrogen bond with a phosphate oxygen that is attached to an isopropyl group.

ClpP's catalytic triad lies in a cleft formed by β strand 4 in the head domain and strand 9 from the handle. This arrangement is reminiscent of the substrate binding pocket in subtilisin, in which two β strands from the enzyme form a three-stranded antiparallel β sheet with a bound substrate (Perona and Craik, 1995). Based upon our preliminary analysis of the ClpP-DFP complex and by analogy with the substrate-binding pocket in subtilisin, we modeled a hepta-peptide, $E^{6}LRWMW^{1}$-$A^{1'}$, into the cleft of the ClpP monomer. In an extended conformation, the model peptide can be oriented to form an antiparallel β sheet with strands 9 and 4 of ClpP. The extent of ClpP's apparent substrate-binding pocket, in the monomer, is defined by the length of β strand 9, to which the backbone atoms of the peptide's P1–P6 residues make hydrogen-bonding interactions with the backbone atoms of the protein (Figure 3C). Oriented in this manner, the substrate Trp, in the P1 position, is located in a deep hydrophobic (S1) pocket and the scissile W^{1}-$A^{1'}$ bond is proximal to the attacking Ser-97 and oxyanion hole. To test our model for substrate binding, we determined the structures of ClpP in complex with the tri-peptide Suc-Leu-Leu-Met-aldehyde (M. Bewley, J. W., J. H., and J. M. F., unpublished data). Preliminary analyses of this structure support the current model.

The Active Sites Are Located in a Central Chamber

Tetradecameric ClpP has an overall cylindrical shape, $\sim$90 Å in both height and diameter, with a central penetrating channel (Figure 4), in agreement with previous structural studies (Flanagan et al., 1995; Kessel et al., 1995). The 14 proteolytic active sites are enclosed within a central, spherical 51 Å chamber formed by the association of the two heptameric rings (Figures 4D and 4E). Access to the chamber from outside is controlled by two axial entrance pores (12 Å long). The pores' interior surface is hydrophilic (Figure 5F) and formed by residues 11–17, whose main-chain atoms lie parallel to the sevenfold axis of the oligomer. Two conserved aromatic residues (Phe-17 in helix A and Phe-49 in helix B) from each subunit are located at the outer periphery of the pores. These residues may play a role in assisting the passage of substrates into, and products out of, the proteolytic

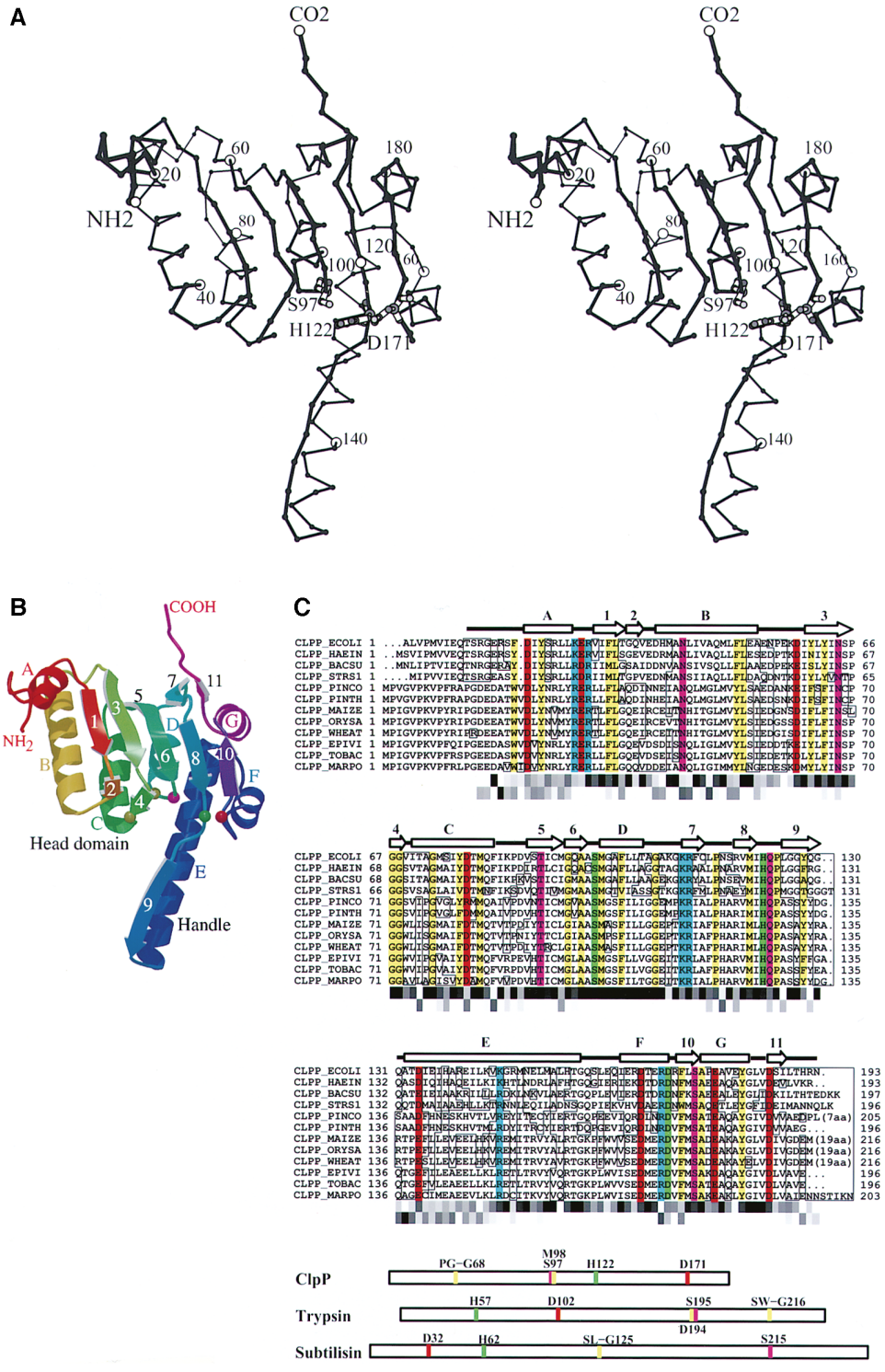

Figure 2. Structure of the ClpP Monomer

(A) A Cα stereodiagram (Priestle, 1988) shows the structure of the ClpP subunit. The amino and carboxyl termini, every 20th Cα, and the catalytic triad (Ser-97, His-122, and Asp-171) are labeled.

(B) A ribbon diagram (Kraulis, 1991) of the ClpP subunit shows its α/β-type fold. The helices and strands are shown from amino to carboxyl terminus with rainbow coloring. In addition, residues in the catalytic triad (Ser-97, magenta; His-122, green; and Asp-171, red) and those that are proposed to stabilize the oxyanion intermediate (Met-98 and Gly-68, olive) are drawn as spheres. In (A) and (B), the seven-fold axis runs in the vertical direction.

(C) A sequence alignment of proteins in the ClpP protease family. Residues in the catalytic triad are shown in green, conserved negatively charged residues in red, conserved positively charged residue in blue, and other conserved residues in yellow; the boxed residues are those that deviate from their consensus sequence (at least six identical or equivalent residues). Shown below the aligned ClpP sequences is a one-

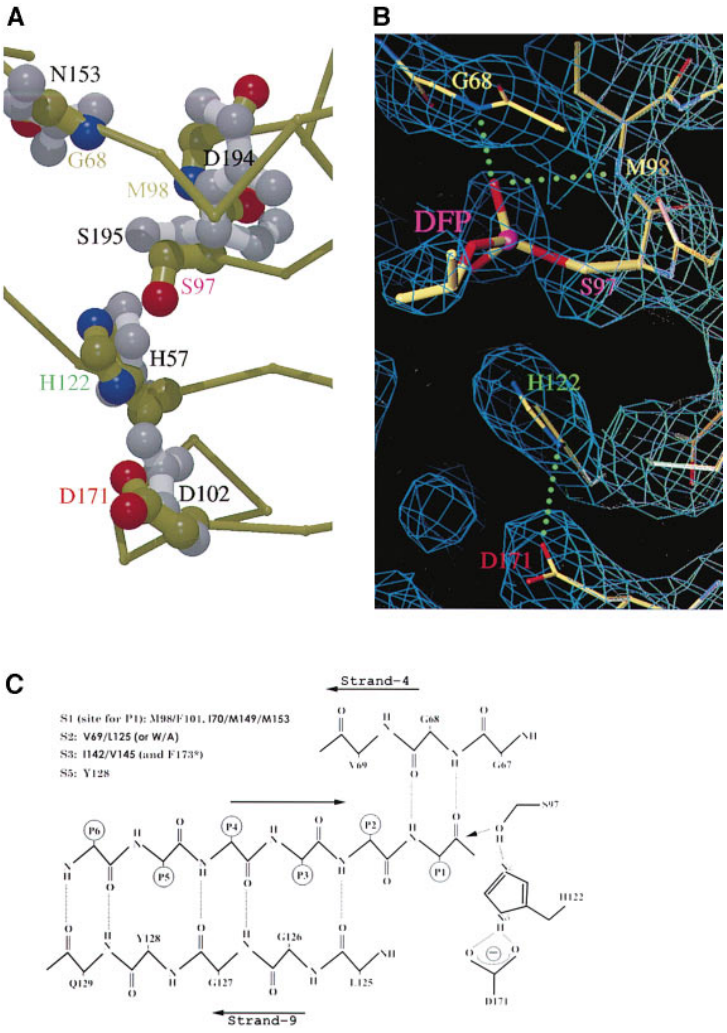

Figure 3. ClpP Has a Conserved Serine-Protease Apparatus

(A) A least-squares superposition between the catalytic triad of ClpP (Asp-171, His-122, and Ser-97) and trypsin (Asp-102, His-57, and Ser-195 in light gray), with the Cα trace of ClpP. The backbone amides of Gly-68 and Met-98 in ClpP, and the backbone amide of Ser-195 and side-chain amine of Asn-153 in trypsin, which participate in stabilizing the putative oxyanion intermediate, are also shown.

(B) A preliminary 2Fo-Fc(apo) Fourier map with the coordinates of the refined structure superimposed at 2.5 Å shows the modification of Ser-97 by di-isopropyl-fluorophosphate. The side chain of Ser-97 is reoriented toward the phosphate atom in DFP to form a covalent bond, while the oxygen of this tetrahedral transition-state analog forms hydrogen bonds with Met-98 and Gly-68.

(C) Schematic representation of the proposed model for substrate binding by ClpP. The hydrogen-bonding network and the hydrophobic contacts between the substrate and surface of the active site cleft are shown. The hepta-peptide substrate (E^6LRWMW^1-$A^{1'}$) binds in a cleft formed by strand 4 in the head domain and strand 9 in the handle of the ClpP subunit. This peptide, in an extended conformation, forms a three-stranded antiparallel β sheet with strands 9 (below) and 4 (above) of ClpP. Included are the hydrophobic residues in the putative S1–S3 and S5 pockets in ClpP that are proposed to interact with the peptide substrate. The residues in the S2 pocket in E. coli ClpP are Val-69/Leu-125; in the plant plastid homologs of ClpP, these residues are W and A, respectively. The asterisk next to Phe-173 of the putative S3 pocket indicates that this residue is from a subunit in the opposing ring. In this figure, the seven-fold axis is oriented along the horizontal axis.

chamber. The solvent-accessible diameter of the pores is ~17 Å near their outer entrance and narrows to ~10 Å at a constriction due to the side-chain atoms of Arg-12, which protrudes into the pore. The side chains of residues 11–17 are built into weak NCS-averaged electron density; thus, the diameter of the constriction may have an error of 1–2 Å. The size of the entrance pores would allow the passage of a β strand, or an α helix (Figure 4F), implying that protein substrates enter the proteolytic chamber in a largely unfolded conformation. The structural features of the entrance pores and proteolytic chamber in ClpP are strikingly similar to those observed in the β-type proteolytic rings of the yeast and T. acidophilum 20S proteosomes and in E. coli HslV (Lowe et al., 1995; Bochtler et al., 1997; Groll et al., 1997), despite their lack of homology to ClpP in primary sequence or secondary and tertiary structure, and may underlie common features in their mechanisms.

We propose that the entrance pores in ClpP will define the hydrodynamic radii of polypeptides that can diffuse freely into and out of the proteolytic chamber, and thus impose strong constraints upon the size and conformation of substrates entering the proteolytic chamber and on the length of products leaving it. Consistent with this hypothesis, ClpP alone efficiently degrades peptides shorter than 6 residues, and more slowly degrades oligopeptides of up to ~30 residues but does not degrade larger oligopeptides and the model protein substrate α casein. (Thompson and Maurizi, 1994; Thompson et al., 1994). Degradation of these larger substrates requires the ATPase components that may unfold and translocate them into ClpP (Gottesman et al., 1997). Mechanistically, the translocation of substrates into the proteolytic chamber may resemble the energy-dependent transport of newly synthesized polypeptides across membranes. Interestingly, ClpC, a Clp ATPase in plants

dimensional representation of the solvent inaccessibility profiles for each residue. Line 1 shows the degree of solvent-inaccessibility resulting from the folding of the monomer, and Line 2 the solvent inaccessibility due to tetradecamer formation. Solvent inaccessibility is represented on a gray scale (black buried, white solvent accessible). Directly below the alignments, the relative positions of the amino acids in the catalytic triad and oxyanion hole of ClpP, trypsin, and subtilisin are shown.

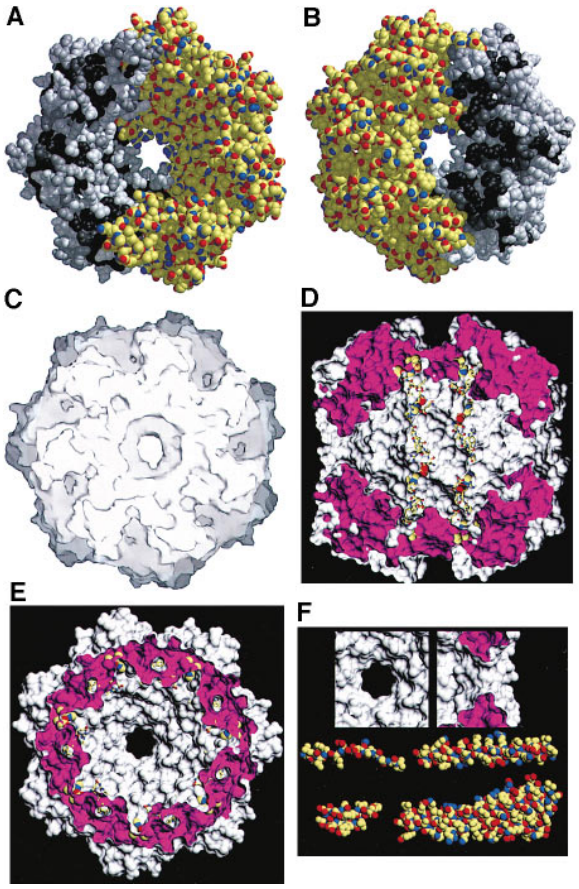

Figure 4. Three-Dimensional Representations of a ClpP Heptamer

(A) Sequence conservation viewed from the inside of the central cavity out along the seven-fold axis (vertical to the page) reveals a patch of conserved residues located at the junction of the head domain and the handle. Part of the model is colored in gray-scale according to sequence conservation (black representing conserved residues) and the remaining sector colored according to atom type (nitrogen, blue; oxygen, red; carbon and sulphur, yellow).

(B) View 180° away from (A) looking from the outside of the cavity in. The most conserved residues are found in the apical surface, where ClpP is thought to interact with the ATPase subunits. The model is colored according to (A).

(C) A surface representation of (B). The most conserved residues lie in grooves on the surface of the molecule.

(D) A longitudinal section of the tetradecamer along a two-fold axis shows the location of the active sites within the large central proteolytic chamber and two elongated pores that restrict access to the chamber. In this representation, the seven-fold axis is aligned vertically. The thin solid walls of the chamber, near the oligomers' equator, are made by the handles of 14 subunits. The catalytic triads are depicted as large spheres, sectioned surfaces are colored magenta, and the modeled hepta-peptide is shown in ball-and-stick representation.

(E) A horizontal section of the tetradecamer in the same orientation as (A) shows the P1 pockets as small circular openings. The coloring is the same as in (D).

(F) A comparison of the pore size with a variety of secondary structural elements. From top to bottom and left to right: two orthogonal views of the entrance pores, β strand 14, α helix P, β strands 21 and 22, and the finger domain (2 α helices) of RB69 DNA polymerase, respectively (Wang et al., 1997).

(Shanklin et al., 1995), has recently been implicated in protein import into chloroplasts (Nielsen et al., 1997).

Surface Properties of ClpP

Each of the three major solvent-exposed surfaces (exterior sides, interior proteolytic chamber, and exterior end-on) of the ClpP oligomer has a distinct character. The exterior side surfaces of ClpP are hydrophilic and composed of nonconserved residues (Figure 4B). The deep notches and grooves in this surface facilitate the tight packing of the oligomers in the crystal. In contrast, the residues contributing to the exposed surface of the proteolytic chamber are partially conserved, presenting ~5500 Å^2 (out of the total 7850 Å^2 of exposed surface area in the cavity) of hydrophobic surface area to the solvent (Figures 4A and 5F). The hydrophobic surfaces in this chamber should be important in maintaining substrates in an unfolded and easily degradable state. Large hydrophobic surfaces are also found in the interior chambers of two other ring-like oligomers: the chaperonin GroEL (Braig et al., 1994; Boisvert et al., 1996), and the 20S proteasome (Lowe et al., 1995; Groll et al., 1997). In all of these oligomers, the ring-like architecture provides a framework to expose large hydrophobic surfaces, while controlling access to these surfaces.

The ATPase components of Clp are thought to bind to the exterior end-on surface of ClpP (Kessel et al., 1995). This surface, viewed looking down the central pore of the oligomer, has a sprocket-like appearance (Figures 4B and 4C) due to seven ridges extending radially outward from the pore's edges. Between the ridges are seven 10 Å–wide grooves, beginning ~54 Å from the pore's center and extending outward for ~20 Å. Their surface is hydrophobic, comprised of conserved and solvent-exposed aromatic residues from strands 1, 3, 5, 7, and 11, and helices B and C including the conserved residues Tyr-60, Tyr-62, and Phe-82. The conserved surfaces of these grooves may stabilize the complexes of ClpP with its ATPase components. The end-on surfaces of the α-subunit rings in the 20S proteasome (Lowe et al., 1995) have a similar sprocket-like appearance, although the role of this surface in the proteasome is not known.

Oligomerization of ClpP

The ClpP protease exists as a tetradecamer, made up of two heptameric rings stacked back-to-back (Figures 4 and 5). The catalytic triad of each subunit is located at the interface between three monomers, and thus oligomerization is required to form the functional protease. The subunit contacts provide a mechanism for communication between active sites that may play a role in the allosteric activation of ClpP. The individual rings are stabilized by extensive interactions among the head domains. In the ClpP oligomer, the amino terminus of each subunit is located inside the cavity near the seven-fold axis; the carboxyl termini (189–193) are at the periphery of the cylinder, lying along the outer surface of helix B of an adjacent subunit. All helices are distributed radially, emanating from the seven-fold axis (Figures 5A and 5B). The close packing of helices B and C from one subunit against the β sheets (strands 1, 3, 5, 7, and 11)

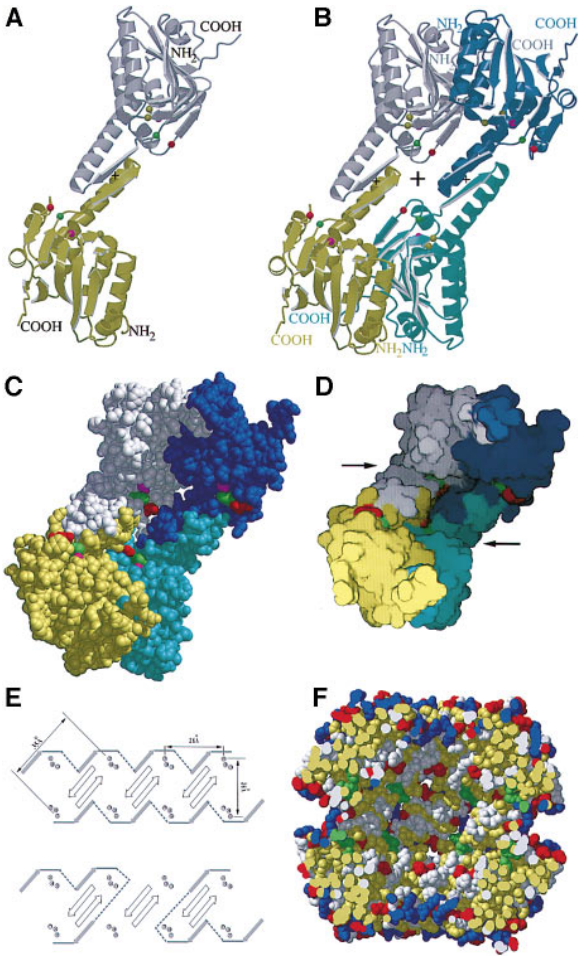

Figure 5. Subunit Interface in ClpP

(A) The intra-ring association of ClpP monomers is shown as a ribbon diagram. Monomer 1 is shown in gray, monomer 2 in olive; residues in the catalytic triad and those that stabilize the oxyanion intermediate are represented as spheres: Ser-97 is magenta, His-122 is green, Asp-171 is red, and Gly-68 and Met-98 are olive. Dimerization of the two rings of heptamers results in the formation of an antiparallel β sheet comprising strand 9 from two NCS-related subunits. The small (+) represents the two-fold axis relating the stacked monomers in opposing rings.

(B) The intraring contacts between monomers are shown; in one ring, monomer 1 (gray) in (A) packs against monomer 3 shown in blue, and in the opposing ring, monomer 2 (olive) in (A) packs against monomer 4 shown in cyan. As in (A), the catalytic residues are shown as spheres. As in (A), the small (+) represents the location of the two-fold axis relating stacked monomers; the large (+) represents the location of a second two-fold axis that lies between each pair of interring subunits.

(C) A CPK representation of (B) showing the interdigitation of the monomers.

(D) A solvent-accessible surface representation of (B) shows the connection between adjacent active site clefts in the heptameric ring. The active sites in opposing heptamers are also connected by channels that lie along the two-fold axes of the oligomer, giving the surface of the proteolytic chamber a zigzag-like appearance.

(E) A schematic representation of two putative models of substrate binding. Strands 9 are drawn as unshaded arrows and heptapeptides as shaded arrows. Dashed lines represent possible connections between hepta-peptides in a continuous substrate. Residues in the catalytic triads are drawn as spheres.

(F) A longitudinal section of a space-filling model colored according to hydrophobicity. The apical and outer equatorial surfaces are enriched in charged residues, whereas the inner surface of the chamber is largely hydrophobic. In this representation, hydrophobic residues (Tyr, Phe, Leu, Ile, Met, Val, Pro, and Ala) are colored in yellow, while charged residues are colored in blue (Lys and Arg) and red (Asp and Glu), respectively. All other residues are colored in gray.

of the next produces alternating layers of helices and sheets around the oligomer, burying 34% of the solvent-accessible surface area of each monomer. The monomer–monomer interface is predominantly hydrophobic (64%), although several hydrogen bonds (Asn-41/Tyr-20, Asn-41/Thr-32, Asp-78/Asn-116, and Asp-171/Try-128) and ion pairs (Arg-118/Glu-141, Arg-170/Glu-134, and Asp-171/His-138) also stabilize the heptamer.

The tetradecamer is formed by the intercalated stacking of the two heptameric rings via their handle domains (Figures 5A–5D and 5F). The interface is stabilized by the formation of hydrogen bonds with the backbone atoms of a two-stranded anti-parallel β sheet (strands 9 from two-fold related subunits). Strand 9 is proposed to be implicated in our model for substrate-binding. The residues in this strand are not conserved, and their side chains do not participate in the two-fold interface or in the model for substrate binding. Stacking of the two heptameric rings buries an additional 8.5% of the solvent-accessible surface area per monomer. Thus, each monomer buries 42.5% (4360 Å^2) of its total surface-accessible area in forming the tetradecamer. Such an extensive subunit interface in ClpP implies that the oligomer provides a rigid scaffold for the proteolytic sites within the central chamber. By comparison, a subunit in the GroEL oligomer, which is thought for functional reasons to be conformationally flexible, contributes only ~6.6% of its surface area toward stabilizing the oligomer (Braig et al., 1994; Boisvert et al., 1996).

Polypeptide Substrate Binding

In the proteolytic chamber of ClpP, perpendicular to the entrance pores, there are two continuous and parallel grooves inscribed around the circumference of its inner walls (Figures 4D and 4E). The grooves are hydrophobic, and each links the active sites in one heptamer ring forming a continuous substrate-binding surface (Figures 4D, 5E, and 5F). Along the grooves, the catalytic triads are spaced ~26 Å (Ser-97Cα-to-Ser-97Cα) apart so that an extended hepta- or octa-peptide substrate can easily span the distance between adjacent active sites. The spatial distribution of active sites in ClpP and the 20S proteasome is nearly identical (Lowe et al., 1995; Groll et al., 1997). Consistent with the previously proposed molecular-ruler model (Wenzel et al., 1994), this arrangement may partly account for the product size distribution of ClpP, which is also centered at hepta- or octa-peptides (Thompson and Maurizi, 1994; Thompson et al., 1994). Polypeptide substrates longer than a single active-site cleft can simultaneously span multiple active sites with segments 8–10 residues in length between adjacent active sites. This model predicts that short peptides would be produced if cleavage occurs nearly simultaneously at adjacent active sites, or if the rate of peptide-bond cleavage is fast compared with the release of products from the substrate binding groove.

The diameter of the entrance pores to the proteolytic chamber will also select for short peptide products, since these can freely diffuse out of the chamber, while larger, partially degraded substrates will be retained. A combination of these two factors may account for the observed distribution of product sizes. Figure 5E is a schematic representation of a polypeptide bound along the continuous intraring groove. The hepta-peptide model only defines the path of each segment's P1-P6 positions, giving no information on residues beyond these positions. Pairs of active sites in opposing heptamers are also connected by interring grooves lying diagonally across the two-fold axis providing a path for substrate exchange between the two heptameric rings. The interring grooves lie adjacent to the end of the antiparallel β sheets formed by strands 9 from two-fold related subunits.

Conclusions

The architecture of the ClpP oligomer (pore size, distribution of the active sites, and the conserved outer end-on surfaces) provides a structural basis for understanding the mechanism of action of ClpP alone, and in the Clp protease. The size of the entrance pores in ClpP define the conformation/size of substrates that can be degraded, while the proteolytic chamber maintains the concentration of active sites (0.35 M) and cleavable peptide bonds in protein substrates translocated into the chamber at similarly high levels. The combination of exposed hydrophobic and hydrogen-bonding (provided by strands 9 and 4) surfaces along the substrate binding grooves may stabilize unfolded substrates in an easily degradable form. Similar surfaces are also seen in the apical substrate binding domain in the chaperone GroEL, which recently was shown to bind substrates in an extended conformation (Buckle et al., 1997). It is not surprising then that protein substrates are degraded completely with little sequence specificity. One major question that remains is how protein substrates are translocated into the proteolytic chamber of ClpP. Based upon the extensive subunit–subunit contacts stabilizing the ClpP oligomer (particularly between the head domains whose packing defines the walls of the entrance pores), it is likely that ClpP plays a passive role in translocation by restricting substrate access and by providing a surface for interaction with the ATPase components. The similarity in architecture of ClpP, HslV, and the 20S proteasomes from Thermoplasma, and yeast, provide support for the notion that these proteases have similar mechanisms of action.

Experimental Procedures

Crystallization and Data Collection

The E. coli ClpP protein was purified as previously described (Flanagan et al., 1995). The initial crystallization condition was found using the Hampton Research sparse matrix screens. Crystals of ClpP were grown at 15°C in sitting drops by mixing equal volumes of a protein solution (10.4 mg/mL in 10 mM HEPES [pH 7.5], 200 mM NaCl, 1 mM DTT) and the well solution (100 mM NaCitrate [pH 5.6], 10% PEG-4000 [w/v], and 20% isopropanol [v/v]). Crystals appeared within 10–24 hr and reached maximum dimensions of ~0.4 mm in each direction. A crystal was taken directly from the mother liquor and frozen in liquid propane prior to low-temperature data collection using a MAR detector on beamline X12C at the Brookhaven National Laboratory, National Synchrotron Light Source. The data were collected in two passes; one pass (HIGHRES) was collected from 41 to 2.2 Å, and the other from 80 to 4.0 Å (LOWRES). For ab initio phase determination, the two data sets were merged (COMBIN). The data were integrated and scaled using the programs DENZO and SCALEPACK (Otwinowski and Minor, 1997), respectively.

Ab Initio Phase Determination Protocol

A self-rotation calculation was performed using the program GLRF (Tong and Rossman, 1990), which revealed the presence of seven-fold noncrystallographic symmetry. Perpendicular to the seven-fold axes were two sets of seven 2-fold axes on the $k = 180^\circ$ section. One set, with lower peak intensities, reflects the molecular symmetry of ClpP; the more intense set is due to intermolecular symmetry of "packing symmetry" (Klug, 1972), which results from a special perpendicular relationship between the crystallographic 2-fold and the 7-fold NCS. The packing symmetry is also present in the related crystal form of ClpP (Shin et al., 1996).

In a previous study, we determined a low-resolution model for the ClpP oligomer from electron micrographs of vanadate-stained particles and solution small-angle scattering (Flanagan et al., 1995), in which ClpP was represented as a hollow cylindrically symmetric particle with inner and outer radii of 17 and 50 Å, respectively, and a height of 80 Å. This low-resolution model was used as a mask to calculate the phases for reflections between 80 and 20 Å resolution. The mask defined the particle's dimensions and its seven-fold NCS, but did not include information about the location of its 2-fold axes. The mask was oriented in the asymmetric unit according to the results of the self-rotation analysis and then positioned according to an overlapping function search (Harada et al., 1981) and visual inspection. The program RAVE (Jones, 1992) was used for NCS averaging and phase extension. Throughout the averaging procedure, the ClpP molecular mask was improved using a maskless averaging procedure, and the matrices were refined using a brute-force search protocol. Details of the structure solution will be presented elsewhere (Wang et al., unpublished data).

Model Building and Refinement

The model contains residues 11–193 for each of the 14 subunits. It was built using O (Jones et al., 1991). The initial model had a working R factor (R_{work}) of 37.7% (R_{free} = 37.5% with 5% of the data) for the data between 5.0 and 2.3 Å, with B factors arbitrarily assigned as 20, 30, and 40 $Å^2$ for the main chain, side chain, and solvent atoms, respectively. This model included residues 11–193, and 89 water molecules per monomer, and had a real-space correlation coefficient of 0.79 between the experimental and calculated densities per residue. The structure was refined using the program X-PLOR version 3.1 (Brünger, 1992). In the early stages of refinement, phases were restrained using the wp weighting scheme and a vector difference minimization (A. Brünger, personal communication), and noncrystallographic symmetry constraints were imposed. Subsequently, NCS restraints were imposed (a weight of 300 for main chain atoms and 200 for side-chain and solvent atoms). The final model has a working R factor of 21.9% (R_{free} of 29.2%) for the data between 80 and 2.3 Å. The coordinates and structure factors for ClpP have been deposited in the Brookhaven Protein Data Bank with accession numbers 1TFY and 1TYFSF, respectively.

Kinetics of Peptide Hydrolysis

The peptidase activity of ClpP was assayed at 25°C by continuously recording the increase in fluorescence due to the release of the 7-amido-4-methyl-coumarin from the dipeptide N-Suc-LY-AMC as described previously (Woo et al., 1989). The reaction was carried out in a buffer consisting of 50 mM Tris–HCl (pH 7.5), 1 mM DTT, 1 mM N-Suc-LY-AMC, and various amounts of purified ClpP or ClpP-D171A. The wavelengths of excitation and emission were 380 and 460 nm, respectively.

Sequence Alignment of ClpP Family Members

The sequence alignment was obtained using the GCG package. Swiss-Prot accession numbers for 12 sequences are ECOLI-P19245, HAEIN-P43867, BACSU-P80244, SRS1-P36398, PINCO-P36387, PINTH-P41609, MAIZE-P26567, ORYSA-P12209, WHEAT-P24064, EPIVA-P30063, TOBAC-P12210, and MARPO-P12208.

Acknowledgments

We thank Drs. T. A. Steitz, R. M. Sweet, D. M. Engelman, J. Shanklin, W. Mangel, and M. C. Bewley for critically reading this manuscript, and R.M. Sweet for helping to collect the low-resolution data essential for this work at X12C beamline, BNL. We would also like to thank Kathleen Griffin for her participation in purifying and assaying ClpP and ClpP-D171A. This work was supported, in part, by the US Department of Energy (contract number DE-AC02-76CH00016 to J. M. F.) and by a National Institutes of Health Grant (GM-22778 to T. A. Steitz).

Received September 19, 1997; revised October 8, 1997.

References

Aizenman, E., Engleberg-Kulka, H., and Glaser, G. (1996). An Escherichia coli chromosomal "addiction module" regulated by 3′,5′-bispyrophosphate: a model for programmed bacterial cell death. Proc. Natl. Acad. Sci. USA *93*, 6059–6063.

Blow, D.M., and Steitz, T.A. (1970). X-ray diffraction studies of enzymes. Annu. Rev. Biochem. *39*, 60–100.

Bochtler, M., Ditzel, L., Groll, M., and Huber, R. (1997). Crystal structure of heat shock locus V (HslV) from Escherichia coli. Proc. Natl. Acad. Sci. USA *94*, 6070–6074.

Boisvert, D.C., Wang, J., Otwinowski, Z., Horwich, A.L., and Sigler, P.B. (1996). The 2.4 Å crystal structure of the bacterial chaperonin GroEL complexed with ATPγS. Nat. Struct. Biol. *3*, 170–177.

Braig, K., Otwinowski, Z., Hedge, R., Boisvert, D.C., Joachimiak, A., Horwich, A.L., and Sigler, P.B. (1994). The crystal structure of the bacterial chaperonin GroEL at 2.8Å. Nature *371*, 578–586.

Brünger, A.T. (1992). X-PLOR version 3.1. A system for X-ray crystallography and NMR (New Haven, CT.: Yale University Press).

Buckle, A.M., Zahn, R., and Fersht, A.R. (1997). A structural model for GroEL-polypeptide recognition. Proc. Natl. Acad. Sci. USA *94*, 3571–3575.

Chen, P., Tsuge, H., Almassy, R.J., Gribskov, C.L., Katoh, S., Vanderpool, D.L., Marosiak, S.A., Pinko, C., Matthews, D.A., and Kan, C.-C. (1996). Structure of the human cytomegalovirus protease catalytic domain reveals a novel serine protease fold and catalytic triad. Cell *86*, 835–843.

Coux, O., Tanaka, K., and Goldberg, A.L. (1996). Structure and functions of the 20S and 26S proteasomes. Annu. Rev. Biochem. *65*, 801–847.

Drenth, J. (1994). Principles of Protein X-Ray Crystallography (New York: Springer-Verlag).

Flanagan, J.M., Wall, J.S., Capel, M.S., Schneider, D.K., and Shanklin, J. (1995). Scanning transmission electron microscopy and small-angle scattering provide evidence that native Escherichia coli ClpP is a tetradecamer with an axial pore. Biochemistry *34*, 10910–10917.

Goldberg, A.L. (1990). ATP-dependent proteases in prokaryotic and eukaryotic cells. Semin. Cell Biol. *1*, 423–432.

Goldberg, A.L. (1992). The mechanism and functions of ATP-dependent proteases in bacterial and animal cells. Eur. J. Biochem. *203*, 9–23.

Goldberg, A.L., Moerschell, R.P., Chung, C.H., and Maurizi, M.R. (1994). ATP-dependent protease La (Lon) from Escherichia coli. Meth. Enzymol. *244*, 350–375.

Gottesman, S. (1996). Proteases: and their targets in Escherichia coli. Annu. Rev. Genet. *30*, 465–506.

Gottesman, S., Clark, W.P., deCrecy-Lagard, V., and Maurizi, M.R. (1993). ClpX, an alternative subunit for the ATP-dependent Clp protease of Escherichia coli. Sequence and in vivo activities. J. Biol. Chem. *268*, 22618–22626.

Gottesman, S., Wickner, S., and Maurizi, M.R. (1997). Protein quality control: triage by chaperones and proteases. Genes Dev. *11*, 815–823.

Groll, M., Ditzel, L., Lowe, J., Stock, D., Bochtler, M., Bartunik, H.D., and Huber, R. (1997). Structure of 20S proteasome from yeast at 2.4 A resolution. Nature *386*, 463–471.

Harada, Y., Lifchitz, A., Berthou, J., and Jolles, P. (1981). A translation function combining packing and diffraction information: an application to lysozyme (high-temperature form). Acta Cryst. *A37*, 398–406.

Holm, L., and Sander, C. (1993). Protein structure comparison by alignment of distance matrices. J. Mol. Biol. *233*, 123–138.

Horwich, A.L. (1995). Molecular chaperones. Resurrection or destruction? Curr. Biol. *5*, 455–458.

Hwang, B.J., Woo, K.M., Goldberg, A.L., and Chung, C.H. (1988). Protease Ti, a new ATP-dependent protease in Escherichia coli contains protein-activated ATPase and proteolytic functions in distinct subunits. J. Biol. Chem. *263*, 8727–8734.

Jones, T.A. (1992). A set of averaging programs. In CCP4 Study Weekend, Molecular Replacement., E.J. Dodson, S. Glover, and W. Wolf, eds. (Daresbury Laboratory, UK: SERC Daresbury Laboratory UK), pp. 91–105.

Jones, T.A., Zhou, J.Y., Cowan, S.W., and Kjeldgaard, M. (1991). Improved methods for building protein models in electron density maps and the location of errors in these models. Acta Cryst. *A47*, 110–119.

Kandror, O., Busconi, L., Sherman, M., and Goldberg, A.L. (1994). Rapid degradation of an abnormal protein in Escherichia coli involves the chaperones GroEL and GroES. J. Biol. Chem. *269*, 23575–23582.

Katayama, Y., Gottesman, S., Pumphrey, J., Rudikoff, S., Clark, W.P., and Maurizi, M.R. (1988). The two-component, ATP-dependent Clp protease of Escherichia coli. Purification, cloning, and mutational analysis of the ATP-binding component. J. Biol. Chem. *263*, 15226–15236.

Kessel, M., Maurizi, M.R., Kim, B., Kocsis, E., Trus, B.L., Singh, S.K., and Steven, A.C. (1995). Homology in structural organization between E. coli ClpAP protease and the eukaryotic 26 S proteasome. J. Mol. Biol. *250*, 587–594.

Klug, A. (1972). Interpretation of the rotation function map of satellite tobacco necrosis virus: octahedral packing of icosahedral particles. Cold Spring Harbor Symp. Quant. Biol. *36*, 483–487.

Kobe, B., and Deisenhofer, J. (1993). Crystal structure of porcine ribonuclease inhibitor, a protein with leucine-rich repeats. Nature *366*, 751–756.

Koster, A.J., Walz, J., Lupas, A., and Baumeister, W. (1995). Structural features of the archaebacterial and eukaryotic proteasomes. Mol. Biol. Rep. *21*, 1–20.

Kraulis, P.J. (1991). MOLSCRIPT: a program to produce both detailed and schematic plots of proteins. J. Appl. Crystallogr. *24*, 946–950.

Laskowski, R.A., MacArthur, M.W., Moss, D.S., and Thornton, J.M. (1993). A program to check the stereochemical quality of protein structures. J. Appl. Cryst. *26*, 283–291.

Lehnherr, H., and Yarmolinsky, M.B. (1995). Addiction protein PhD of plasmid prophage P1 is a substrate of the ClpXP serine protease of Escherichia coli. Proc. Natl. Acad. Sci. USA *92*, 3274–3277.

Levchenko, I., Luo, L., and Baker, T.A. (1995). Disassembly of the Mu transposase tetramer by the ClpX chaperone. Genes Dev. *9*, 2399–2408.

Lowe, J., Stock, D., Jap, B., Zwickl, P., Baumeister, W., and Huber, R. (1995). Crystal structure of the 20S proteasome from the Archaeon T. acidophilum at 3.4 Å resolution. Science *268*, 533–539.

Lupas, A., Flanagan, J.M., Tamura, R., and Baumeister, W. (1997). Self-compartmentalizing proteases. Trends Biochem. Sci., in press.

Matthews, B.W. (1968). Solvent content of protein crystals. J. Mol. Biol. *33*, 491–497.

Maurizi, M.R. (1992). Proteases and protein degradation in Escherichia coli. Experientia *48*, 178–201.

Maurizi, M.R., Clark, W., Kim, S.H., and Gottesman, S. (1990). Clp P represents a unique family of serine proteases. J. Biol. Chem. *265*, 12546–12552.

Maurizi, M.R., Thompson, M.W., Singh, S.K., and Kim, S.-H. (1994). Endopeptidase Clp: ATP-dependent Clp protease from Escherichia coli. Meth. Enzymol. *244*, 315–331.

Nielsen, E., Akita, M., Davila-Aponte, J., and Keegstra, K. (1997). Stable association of chloroplastic precursors with protein-translocation complexes containing proteins from both envelope membranes and a stromal Hsp100 molecular chaperone. EMBO J. *16*, 935–946.

Otwinowski, Z., and Minor, W. (1997). Processing of X-ray diffraction data collected in oscillation mode. Meth. Enzymol. *276*, 307–326.

Perona, J.J., and Craik, C.S. (1995). Structural basis of substrate specificity in the serine proteases. Prot. Sci. *4*, 337–360.

Priestle, J.P. (1988). RIBBON: a stereo cartoon drawing program for proteins. J. Appl. Cryst. *21*, 572–576.

Rohrwild, M., Pfeifer, G., Santarius, U., Muller, S.A., Huang, H.C., Engel, A., Baumeister, W., and Goldberg, A.L. (1997). The ATP-dependent HslUV protease from Escherichia coli is a four-ring structure resembling the proteasome. Nat. Struct. Biol. *4*, 133–139.

Schweder, T., Lee, K.H., Lomovskaya, O., and Matin, A. (1996). Regulation of Escherichia coli starvation sigma factor (sigma s) by ClpXP protease. J. Bacteriol. *178*, 470–476.

Shanklin, J., DeWitt, N.D., and Flanagan, J.M. (1995). The stroma of higher plant plastids contain ClpP and ClpC, functional homologs of Escherichia coli ClpP and ClpA: an archetypal two-component ATP-dependent protease. Plant Cell *7*, 1713–1722.

Shin, D.H., Lee, C.S., Chung, S.H., and Suh, S.W. (1996). Molecular symmetry of the ClpP component of the ATP-dependent Clp protease, an Escherichia coli homolog of 20S proteasome. J. Mol. Biol. *262*, 71–76.

Squires, C., and Squires, C.L. (1992). The Clp proteins: proteolysis regulators or molecular chaperones? J. Bacteriol. *174*, 1081–1085.

Steitz, T.A., and Shulman, R.G. (1982). Crystallographic and NMR studies of the serine proteases. Annu. Rev. Biophys. Bioeng. *11*, 419–444.

Thompson, M.W., and Maurizi, M.R. (1994). Activity and specificity of Escherichia coli ClpAP protease in cleaving model peptide substrates. J. Biol. Chem. *269*, 18201–18208.

Thompson, M.W., Singh, S.K., and Maurizi, M.R. (1994). Processive degradation of proteins by the ATP-dependent Clp protease from Escherichia coli. Requirement for the multiple array of active sites in ClpP but not ATP hydrolysis. J. Biol. Chem. *269*, 18209–18215.

Tobias, J.W., Shrader, T.E., Rocap, G., and Varshavsky, A. (1991). The N-end rule in bacteria. Science *254*, 1374–1377.

Tomoyasu, T., Gamer, J., Bukau, B., Kanemori, M., Mori, H., Rutman, J.A., Oppenheim, B.A., Yura, T., Yamanaka, K., Niki, H., Hiraga, S., and Ogura, T. (1995). Escherichia coli FtsH is a membrane-bound, ATP-dependent protease which degrades the heat-shock transcription factor sigma-32. EMBO J. *14*, 2551–2560.

Tong, L., and Rossman, M.G. (1990). The locked rotation function. Acta Cryst. *A46*, 783–792.

Wang, J., Sattar, A.K., Wang, C.C., Karam, J.D., Konigsberg, W.H., and Steitz, T.A. (1997). Crystal structure of a pol alpha family replication DNA polymerase from bacteriophage RB69. Cell *89*, 1087–1099.

Wawrzynow, A., Banecki, B., and Zylicz, M. (1996). The Clp ATPases define a novel class of molecular chaperones. Mol. Microbiol. *21*, 895–899.

Wawrzynow, D., Wojtkowiak, D., Marzsalek, J., Banecki, B., Jonsen, M., Graves, B., Georgopoulos, C., and Zylicz, M. (1995). The ClpX heat-shock protein of Escherichia coli, the ATP-dependent substrate specificity component of the ClpP-ClpX protease, is a novel molecular chaperone. EMBO J. *14*, 1867–1877.

Wenzel, T., Eckerskorn, C., Lottspeich, F., and Baumeister, W. (1994). Existence of a molecular ruler in proteasomes suggested by analysis of degradation products. FEBS Lett. *349*, 205–209.

Wickner, S., Gottesman, S., Skowyra, D., Hoskins, J., McKenney, K., and Maurizi, M.R. (1994). A molecular chaperone, ClpA, functions like DnaK and DnaJ. Proc. Natl. Acad. Sci. USA *91*, 12218–12222.

Wojtkowiak, D., Georgopoulos, C., and Zylicz, M. (1993). Isolation and characterization of ClpX, a new ATP-dependent specificity component of the Clp protease of Escherichia coli. J. Biol. Chem. *268*, 22609–22617.

Woo, M.K., Chung, W.J., Ha, D.B., Goldberg, A.L., and Chung, C.H. (1989). Protease Ti from Escherichia coli requires ATP hydrolysis for protein breakdown but not for hydrolysis of small peptides. J. Biol. Chem. *264*, 2088–2091.